Lab on a Chip

PAPER

View Article Online
View Journal | View Issue

Check for updates

Cite this: *Lab Chip*, 2017, **17**, 3168

Multiplex coaxial flow focusing for producing multicompartment Janus microcapsules with tunable material compositions and structural characteristics†

Qiang Wu,‡[a] Chaoyu Yang,‡[a] Guangli Liu,[a] Wanghuai Xu,[a] Zhiqiang Zhu,[a] Ting Si *[b] and Ronald X. Xu*[ac]

Received 22nd July 2017,
Accepted 9th August 2017

DOI: 10.1039/c7lc00769h

rsc.li/loc

We propose a simple but efficient multiplex coaxial flow focusing (MCFF) process for single-step fabrication of multicompartment Janus microcapsules (MJMs) in a wide range of operating parameters. The produced MJMs consist of a multicompartmental core–shell structure with material compositions tunable in individual shell and core compartments. Potential applications of such a MJM agent are demonstrated in both benchtop and *in vitro* experiments. For the benchtop experiment, magnetic nanoparticles are loaded into one of the shell compartments and photopolymerized under ultraviolet light for controlled alignment and rotation of the microcapsules in a magnetic field. For the *in vitro* experiment, four different types of cells are encapsulated in the desired compartments of sodium alginate MJMs and co-cultured for seven days. By increasing the number of coaxial needles, we are also able to produce MJMs with three or more compartments. Our studies have shown that the proposed MCFF process is able to produce MJMs with desired material compositions and narrow size distribution. This process is inexpensive and scalable for mass production of various MJMs in its potential applications in biomedical imaging, drug delivery, and regenerative medicine.

Introduction

In recent years, microfabrication of complex emulsions such as Janus droplets[1–3] and multicompartment emulsions[4,5] has attracted more and more research interest. Janus droplets can exhibit two or more distinct chemical or physical properties due to their special structures. Multicompartment emulsions are emulsions that encapsulate core drops of multiple components in their shell materials. These emulsions have great potential in various applications, such as remote manipulation,[6] photonic devices,[7,8] sensors,[9] drug release[10] and other biomedical and clinical applications.[11–14] Previously used processes for producing these complex emulsions include microfluidic devices,[15–18] phase separation,[19,20] electrospray[21] and modified double emulsification.[22,23] In the present work, the motivation is to produce multicompartment Janus microcapsules (MJMs) that can combine the advantageous features of Janus droplets and multicompartment emulsions with precise control of both size and structural characteristics. This type

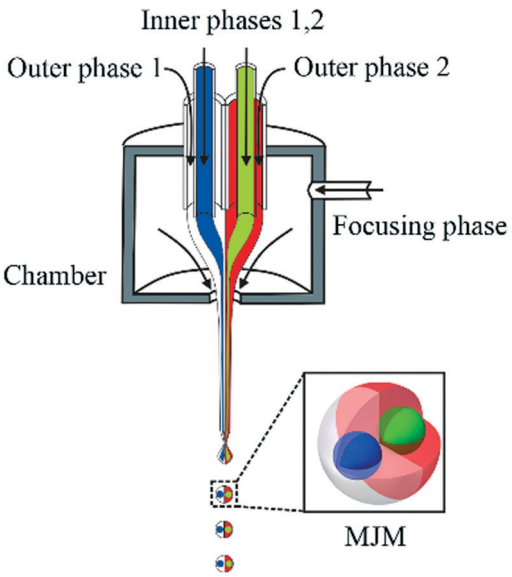

Fig. 1 Schematic of the experimental setup for producing MJMs by the MCFF process.

[a] *Department of Precision Machinery and Precision Instrumentation, University of Science and Technology of China, Hefei, Anhui 230026, PR China*
[b] *Department of Modern Mechanics, University of Science and Technology of China, Hefei, Anhui 230026, PR China. E-mail: tsi@ustc.edu.cn*
[c] *Department of Biomedical Engineering, The Ohio State University, Columbus, OH 43210, USA. E-mail: xu.ronald@hotmail.com; Fax: +1 614 292 7301*

† Electronic supplementary information (ESI) available: ESI (S1): the 3D stereogram of a MJM; ESI (S2): the translational movement of a magnetic MJM; ESI (S3): the rotational motion of a magnetic MJM; ESI (S4): the 3D stereogram of the three-core–compartment microcapsules. See DOI: 10.1039/c7lc00769h

‡ These authors contributed equally to this work.

of emulsion is of great importance in practical applications. For example, it is desirable to achieve optimized dosimetry and precisely controlled release of multiple therapeutic components in personalized medicine.

Recently, Choi *et al.*[24] and Zarzar *et al.*[25] have fabricated complex emulsions based on a phase separation technique, and the process feasibility was highly dependent on the physical and chemical characteristics of the working materials. Lee *et al.*[26] and Shang *et al.*[17] have produced multicompartment emulsions using capillary array injection microfluidic devices, and the competitive wetting of confined channel walls exists in the process. Therefore, reliable mass production of MJMs by previously reported methods is still challenging. Here, we report a simple but efficient multiplex coaxial flow focusing (MCFF) method for one-step fabrication of MJMs with high throughput in a wide range of material properties. The proposed MCFF process, as illuminated in Fig. 1, can be characterized by the formation of steady liquid jets and the breakup of these jets into droplets due to the instability mechanism.[27,28] This method originates from gas-driven[29,30] and liquid-driven[31] flow focusing processes, but the device geometries and the flow patterns among them are completely different. The MCFF process has a more advanced experimental set up for the production of MJMs with designated structures and functions. In comparison with other processes that rely on planar PDMS microchannels and glass microcapillaries, the MCFF process is able to avoid the capillarity and wetting effects of boundary walls and boost liquid flow rates by hundreds of folds, leading to dramatically increased productivity. The flow velocities of both continuous and dispersed phases in the MCFF method are relatively high, resulting in a moderate Reynolds number. Since the MCFF process is able to overcome the viscous effects in individual devices and reduce the structural heterogeneity, it is technically feasible to scale it up for mass production of MJMs in an industrial setting. Furthermore, unlike other processes that produce droplets in constrained spaces, the MCFF process produces MJMs in an open space, making it easy to automate particle solidification, collection, and further post processing.

By manipulating the liquid flow rates and material combinations, we are able to produce different types of complex emulsions by directly using the same experimental platform. In this work, several experiments have been performed to demonstrate the advantages of the MCFF method. The generated MJMs can be solidified by ultraviolet (UV) light to produce drug-laden particles with controllable size, internal structure and morphological characteristics. The sodium alginate MJMs provide an effective platform for three-dimensional cell co-culture. In addition, increasing the number of coaxial needles in the MCFF device may yield MJMs with multiple compartments.

Experimental methods

Experimental setup for the MCFF process

Typically, MJMs are configured as microcapsules of two or more materials that encapsulate compartments of different materials. In order to fabricate MJMs with such a configuration, we have designed a MCFF assembly consisting of two coaxial needles joined parallel by laser welding, as described before.[31,32] The coaxial needles consist of an inner needle (inner diameter: 0.26 mm, outer diameter: 0.49 mm) and an outer needle (inner diameter: 0.84 mm, outer diameter: 1.27 mm). All the tips and edges of the needles are rounded in order to minimize the influence of undesirable disturbances. The coaxial needles are completely sealed and their concentricity is carefully maintained to ensure a steady fluid supply and uniform flow field. Two or more coaxial needles with the same geometric features are aligned in parallel and welded together to form the final needle assembly. The needle assembly is mounted in a pressure chamber with its exit facing a small orifice (diameter: 0.4 mm) located at the centre of a thin glass plate. The vertical distance from the thin glass plate to the tip of the inner needle is adjusted to be 1.5 mm. Five channels of syringe pumps (Pump33, Harvard Apparatus, Holliston, MA) are used to provide continuous flows of two inner phases, two outer phases and the focusing phase. The fluid dynamics in the MCFF process is monitored by a CCD camera (Allied Vision Technologies) equipped with a microscope lens in real time under illumination of a strobe flashlight (flashing frequency: 3.2 kHz) from the other side of the device. MJMs are photopolymerized in a UV irradiation zone generated by UV light (De Sheng Xing Electronics Co. Ltd., China, UVP60, 365 nm, 8.8 W/cm2). Images of MJMs are captured using a Nikon T2000 inverted microscope (Nikon, Japan) equipped with a CCD camera. Fig. 1 shows the basic experimental setup for the MCFF process. As the fluids pass through the orifice, a multiphase cone–jet structure surrounded by the focusing fluid is formed and the jet eventually breaks up into droplets due to the perturbation propagation along the jet surface. The breakup status of the multiphase liquid jet is heavily dependent on the inner, outer and focusing liquid flow rates, similar to that in single and coaxial flow focusing processes.[30,33] This MCFF assembly is simple, inexpensive, and can be readily scaled up for mass production in an industrial setting.

Reagents

To demonstrate the capability of the MCFF method to produce MJMs, various combinations of the inner and the outer fluids are tested. In the first test, the two outer phases are the photocurable organic material ethoxylated trimethylolpropane triacrylate (ETPTA, Aldrich, ρ = 1.11 g cm^{-3}, μ = 0.061 Pa s, σ = 34.0 mN m^{-1}) resin mixed with 2% photoinitiator 2-hydroxy-2-methylphenylpropanone (Aldrich), where ρ, μ, and σ are the density, viscosity and surface tension of liquids, respectively. One portion of ETPTA is stained with red dye to facilitate better visualization of the fluid interfaces. In order to achieve better mixing, ETPTA is premixed with ethanol in equal volume, followed by the addition of the photoinitiator at a volume fraction of 2%. The mixture is placed in an oven for 12 h at 70 °C to promote complete volatilization of ethanol. The two inner phases are 10 wt%

poly(vinyl alcohol) (PVA; Mw: 13 000–23 000 g mol^{-1}, 87–89% hydrolyzed, Sigma-Aldrich, St. Louis, MO) solution (ρ = 1.09 g cm^{-3}, μ = 0.015 Pa s, σ = 41.5 mN m^{-1}). For the experiment of fabricating MJMs, the focusing aqueous phase is 2 wt% PVA solution (ρ = 1.02 g cm^{-3}, μ = 0.002 Pa s, σ = 35.9 mN m^{-1}). Trimethylolpropane triacrylate (TMPTA) is supplied by Sigma Aldrich. In the second test, sodium alginate MJMs are produced for co-culturing of different cells. In this case, the focusing phase is mineral oil (ρ = 0.85 g cm^{-3}, μ = 0.050 Pa s, σ = 31.2 mN m^{-1}), the outer phases are 2 wt% sodium alginate solution (ρ = 1.05 g cm^{-3}, σ = 45.9 mN m^{-1}) mixed with different types of cells, the inner phases are 1 wt% sodium alginate solution (ρ = 1.02 g cm^{-3}, σ = 54.1 mN m^{-1}) mixed with different types of cells, and the collection liquid is 2 wt% calcium chloride solution. Four kinds of cells are used in the experiment. The fluorescence images are taken by laser scanning confocal microscopy (Nikon, Ti-E). Ultrapure deionized water is generated by a Nanopure Infinity water purification system (Millipore, Direct-Q 3). All experiments are performed at room temperature.

Results and discussion

MCFF fabrication of MJMs

In this work, the resultant microdroplets are generated at a nearly constant frequency and are further photopolymerized under UV light to form the MJMs. The size and uniformity of the MJMs can be determined by changing the liquid flow rates in the MCFF process. The stability of the cone should be maintained in order to achieve the steady emission of thin liquid jets from the tip of the cone. In the beginning, we study the effects of flow rates of the focusing phase (Q_f) on the morphology of the cone–jet configurations by keeping the other parameters constant. Here, the moderate volumetric flow rates of two inner and two outer phases are chosen to be $Q_{i1} = Q_{i2}$ = 3 ml h^{-1} and $Q_{o1} = Q_{o2}$ = 20 ml h^{-1}, respectively. As Q_f reaches 300 ml h^{-1}, the compound microdroplets can be obtained from the tip of the steady cone in a dripping mode. In this case, the viscous shear force is weak so that the inner and the outer phases maintain nearly spherical shapes because of the surface/interface tension. The dripping mode appears in a narrow range of Q_f and the produced microdroplets have a uniform but very large size. As the amplitude of Q_f increases to 400 ml h^{-1}, the mode turns into an axisymmetric jetting mode. In this mode, a straight multiphase liquid jet is smoothly issued from the tip of the steady cone. When the wavy amplitude on the jet interface is continuously amplified, the jet breaks up. In experiments, the interfaces between two inner, two outer and focusing phases can be clearly identified, as shown in Fig. 2(a). Two outer liquid jets surrounding two inner liquid threads move in a straight line with almost constant diameter and eventually break up into microdroplets with uniform size distribution and a satisfactory morphology in the regime of the Rayleigh instability.[29,30,33] It can be easily seen that the inner phases are completely encapsulated within the outer phases,

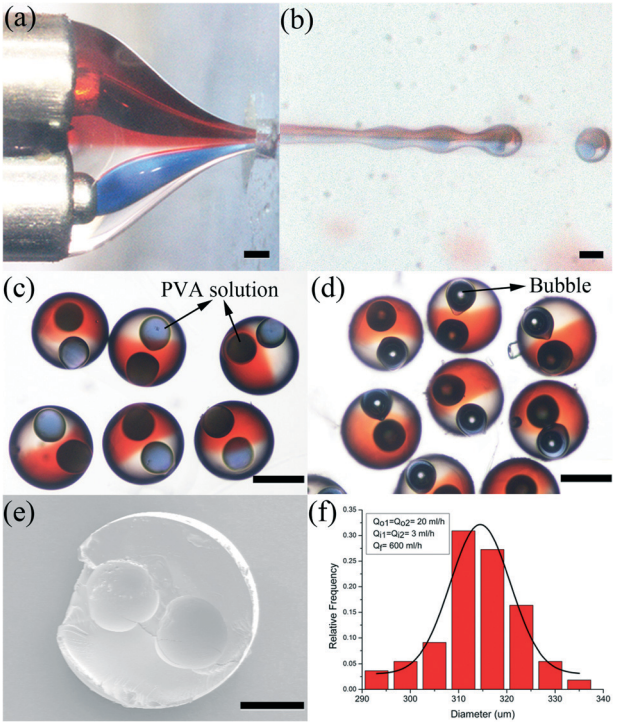

Fig. 2 Illustration of the MCFF process and the characteristics of the produced MJMs: microscopy images of (a) a steady cone–jet mode in the MCFF process, (b) breakup of the multiphase liquid jet, (c) the morphology of collected MJMs and (d) the occurrence of cavitation within MJMs (scale bar: 200 μm). (e) The SEM image of a MJM (scale bar: 100 μm); (f) the size distribution of MJMs. The liquid flow rates: $Q_{i1} = Q_{i2}$ = 3 ml h^{-1}, $Q_{o1} = Q_{o2}$ = 20 ml h^{-1} and Q_f = 600 ml h^{-1}.

indicating no leakage of the inner materials. Fig. 2(b) shows the breakup of the multiphase liquid jets into microdroplets. The axisymmetric jetting mode in the MCFF process is able to maintain the steady cone–jet configuration in a wide range of process parameters. The amplitude of Q_f can be up to 2000 ml h^{-1} and the resultant MJM size can be controlled quantitatively by adjusting the liquid flow rates of the inner and outer phases. As Q_f increases, the size of the steady cone and jet decreases, resulting in the MJMs with smaller size and wider size distribution.

In this work, all the MJMs are generated in the axisymmetric jetting mode. The volumetric flow rates of two inner (Q_{i1}, Q_{i2}), two outer (Q_{o1}, Q_{o2}), and focusing (Q_f) streams are $Q_{i1} = Q_{i2}$ = 3 ml h^{-1}, $Q_{o1} = Q_{o2}$ = 20 ml h^{-1}, and Q_f = 600 ml h^{-1}, respectively. The polymeric shell of MJMs is solidified by UV light illumination for 3 s after collection. Fig. 2(c) shows the optical microscopy image of the collected MJMs. According to the figure, the interfaces between the two outer solidified ETPTA phases and core–shell structures of the MJMs can be identified. In addition, two inner liquid droplets are located on the opposite sides of the MJMs, as evidenced in a video clip in the ESI† (S1). Interestingly, cavitation of MJMs can be achieved based on the semipermeability of solid shells,[34] and the morphology of these MJMs is presented in Fig. 2(d). The SEM image in Fig. 2(e) shows the cross-sectional view of a resultant MJM after polymerization. Under the experimental

conditions, the produced MJMs have a mean diameter of 313.5 μm with a standard deviation of 8.2 μm, and the polydispersity index is 2.6%, as plotted in Fig. 2(f). The droplet generation frequency of this process is estimated to be around 1×10^3 Hz, which is superior to those of many other microfluidic processes whose production rates range from several to dozens of droplets per second.[17,26,35] The high throughput indicates the advantage of the MCFF process, which is determined by the following characteristics. First, the surrounding drive fluid streams keep the dispersed fluids away from the boundary walls of the device and prevent the wetting and capillarity effects. Second, the liquid flow rates in this method can be greater than those in planar PDMS microchannels and glass microcapillaries by several hundred folds, leading to significantly greater productivity. Third, the MCFF process involves multiplex flows with high velocities and the resultant large Reynolds numbers may effectively overcome the structural heterogeneity due to the viscous effects. Therefore, the MCFF method can be easily scaled up for industrial applications.

Additionally, it is technically feasible to tune the internal topological structure of the produced microcapsules without changing the experimental setup, as shown in Fig. 3. As one of the inner phases is turned off, the MCFF process produces Janus microparticles with double emulsion in one hemisphere only, as shown in Fig. 3(a)–(d). As all of the inner phases are turned off, the process produces traditional Janus microparticles, as displayed in Fig. 3(e) and (f). In addition, the multicompartment double emulsions can be generated by employing the same outer phases, as illuminated in Fig. 3(g) and (h). Furthermore, MJMs with two different outer materials can be fabricated by replacing one of the outer oil phases with trimethylolpropane triacrylate (TMTPA). Fig. 3(i) and (j) show the steady cone and the produced MJMs. These results imply that the MCFF process is able to produce complex emulsions with tunable internal topological structures within one step by adjusting the process parameters without changing the geometry of the device.

As demonstrated in our experiments, the MCFF process is able to maintain the steady cone–jet configuration in a wide range of process parameters, and the resultant MJM size can be controlled quantitatively by adjusting the liquid flow rates. Fig. 4(a) and (b) show the relationships between the diameters of the produced MJMs and the liquid flow rates of different phases in the axisymmetric jetting mode. The diameter of MJMs increases as the value of $Q_{o1} + Q_{o2}$ increases and decreases as the value of Q_f increases. The correlation between the resultant particle size and the process parameters follows a scaling law, as shown below,

$$D \sim \alpha[(Q_{i1} + Q_{i2} + Q_{o1} + Q_{o2})/Q_f]^{1/2} D_{orif}, \quad (1)$$

where D and D_{orif} are the diameters of the droplet and the orifice, respectively; α is a constant that is mainly dependent on the flow modes of the jet breakup. Good agreement is achieved between the experimental and theoretical results for a given $\alpha = 2.84$ (Fig. 4). The results further verify the quantitative control of the MCFF process and provide theoretical guidance for practical applications, as demonstrated below with magnetic MJMs and MJMs with co-cultured cells.

Fabrication of magnetic MJMs

In the MCFF process, magnetic MJMs can be directly fabricated by incorporating modified ferroferric oxide (Fe_3O_4) nanoparticles into one of the oil phases. Due to the advantageous feature of the MCFF device that the inner and outer fluids are not in contact with solid walls, the Fe_3O_4 nanoparticles can be thoroughly dispersed into the MJMs without any adhesion to the device boundaries. In this work, Fe_3O_4 nanoparticles are synthesized in advance by following an established protocol.[36] In order to produce the MJMs with heterogeneity, 2 wt% Fe_3O_4 nanoparticles are only dispersed in one outer oil phase of ETPTA. The liquid flow rates are kept independently at $Q_{i1} = Q_{i2} = 3$ ml h^{-1}, $Q_{o1} = Q_{o2} = 20$ ml h^{-1}, and $Q_f = 600$ ml h^{-1}, respectively. The images of the

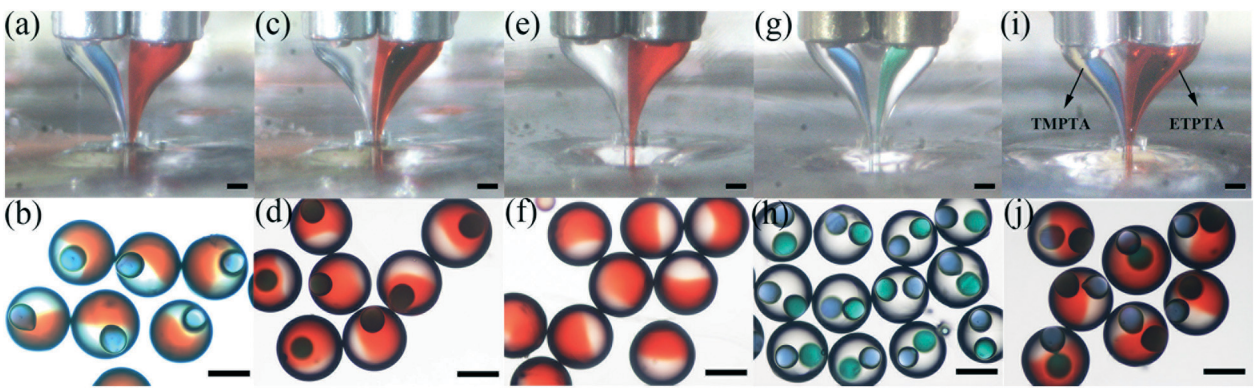

Fig. 3 Production of complex emulsions with tunable internal topological structures by adjusting the process parameters in the same device (scale bars: 200 μm): microscopy images of the steady cone–jet mode (top) and the collected MJMs (bottom) for (a and b) $Q_{i1} = 0$ and $Q_{i2} = 3$ ml h^{-1}, (c and d) $Q_{i1} = 3$ ml h^{-1} and $Q_{i2} = 0$, (e and f) $Q_{i1} = Q_{i2} = 0$, (g and h) $Q_{i1} = Q_{i2} = 3$ ml h^{-1} without dyes inside the outer phases, and (i and j) $Q_{i1} = Q_{i2} = 3$ ml h^{-1} with two kinds of outer materials. The rest of the liquid flow rates: $Q_{o1} = Q_{o2} = 20$ ml h^{-1}, and $Q_f = 600$ ml h^{-1}.

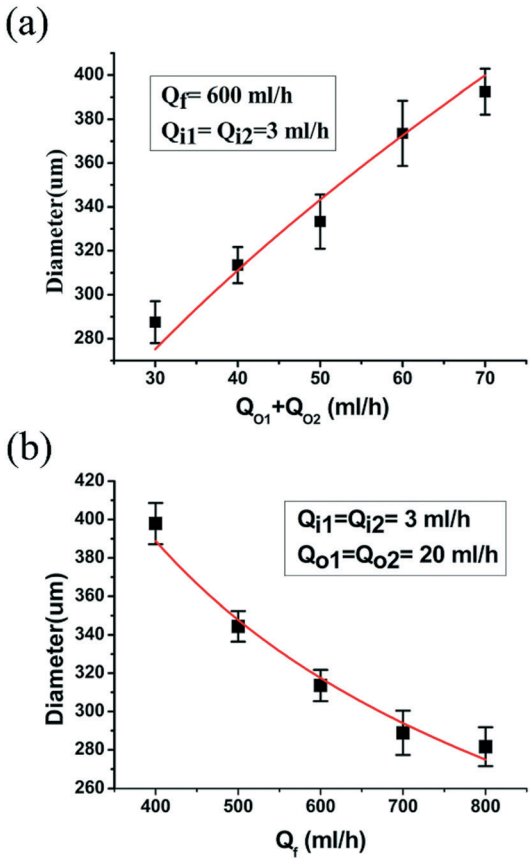

Fig. 4 The relationships of MJM diameter with (a) Q_{o1} + Q_{o2} and (b) Q_f in experimental measurements compared with the scaling law predictions (solid lines).

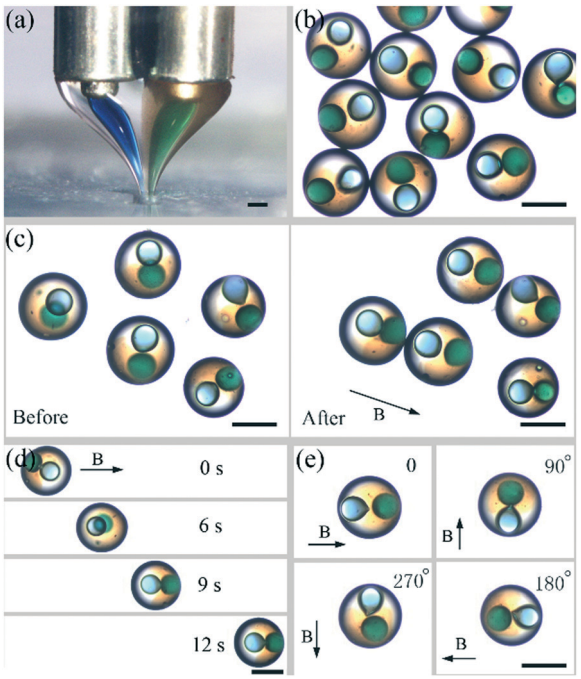

Fig. 5 Fabrication of the magnetic MJMs by incorporating Fe_3O_4 nanoparticles in one of the oil phases (scale bars: 200 μm): microscopy images of (a) the stable cone–jet mode in the MCFF process, (b) the morphology of the produced magnetic MJMs, (c) the alignment of the MJMs under a directional magnetic field, (d) the translational motion of a MJM toward the magnet, and (e) the rotational motion of a MJM.

steady compound cone and the produced magnetic MJMs are shown in Fig. 5(a) and (b). According to the figures, the interface boundaries are clearly visible in the steady cone and the resultant magnetic MJMs have a uniform size distribution.

As the Fe_3O_4 nanoparticles are dispersed in one hemisphere of the MJMs, the resultant magnetic field distribution is asymmetric, enabling the controlled motion of the MJMs in an external magnetic field. Fig. 5(c) shows that all magnetic MJMs in arbitrary directions can be forced to point to the same direction in a stationary magnetic field. A video clip in the ESI† (S2) further demonstrates precise manipulation of an initially static magnetic MJM by a small magnet. As the magnet moves to the vicinity of the MJM, two internal compartments of the MJM re-orientate and the magnetic compartment drives the translation of the MJM. In Fig. 5(d), microscopy images of the magnetic MJM during its motion toward the magnet are acquired at different moments. Additionally, the rotational motion of the magnetic MJM can also be observed by changing the position of the magnet, and the orientation of two internal compartments can be controlled precisely, as captured shown in a video clip in the ESI† (S3). In Fig. 5(e), microscopy images of the magnetic MJM are acquired during its rotational motion as the direction of the magnetic field is controlled at 0, 90, 180 and 270 degrees, respectively. This method enables the encapsulation of different material compositions in the core compartments of the magnetic MJMs, leading to many significant applications in drug delivery,[37,38] bead manipulation[15,39] and biological imaging.[40,41]

Fabrication of sodium alginate MJMs for 3D cell co-culture

For *in vitro* demonstration of the MJM applications, four kinds of viable cells are encapsulated in the sodium alginate MJMs for 3D co-culture. The two outer phases are 2 wt% sodium alginate mixed with HUVEC cells (stained with DiO dye) and HL7702 cells, respectively. The two inner phases are 1 wt% sodium alginate mixed with LX2 cells (stained with DiI dye) and HepG2 cells (stained with Hoechst dye), respectively. The cell concentration is about 3.3×10^6 per millilitre. The focusing phase is mineral oil. A beaker containing an aqueous solution of 2.0 w/v% calcium chloride is placed underneath the MCFF device in order to collect the produced droplets to form MJMs. The experimental system and materials are sterilized in an autoclave before experiment. The volumetric flow rates of the two inner, two outer, and focusing streams are 3 ml h^{-1}, 12 ml h^{-1}, and 600 ml h^{-1}, respectively.

As the produced alginate MJMs are collected by the calcium chloride solution, the calcium ions cause rapid gelation of the sodium alginate shell. The mixture with alginate MJMs are centrifuged to remove oil and $CaCl_2$ solution, and then washed with 0.9% NaCl solution several times. Finally, the

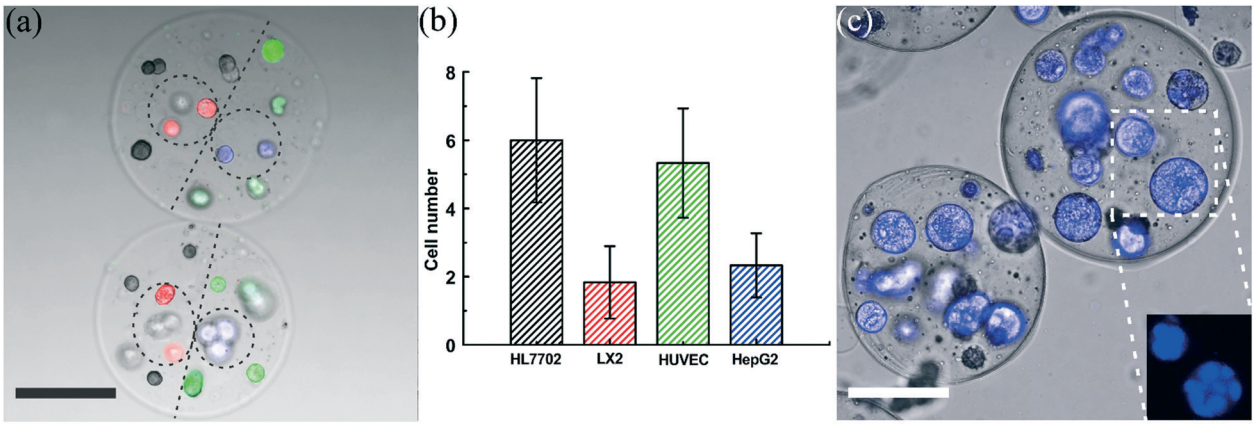

Fig. 6 3D co-culture of multiple types of cells in sodium alginate MJMs (scale bars: 100 μm). (a) Fusion of bright field and fluorescence images of MJMs that encapsulate four types of cells in the designated compartments. The cells are stained in red, blue and green, respectively. (b) The average numbers of four different cells encapsulated in each MJM. (c) Fusion of bright field and fluorescence images of the cell-loaded sodium alginate MJMs after 7 days of co-culture. Lower-right is the fluorescence image that shows individual cells within the MJMs.

produced alginate MJMs are put into an incubator to co-culture for several days. Fig. 6(a) shows the fusion of bright field and fluorescence images for the produced sodium alginate MJMs. According to the different colours in the image, four kinds of viable cells encapsulated in the sodium alginate MJMs can be identified. The LX2 and HepG2 cells are loaded into two different cores on the opposite sides of the MJMs, surrounded by HL7702 cells and HUVEC cells, respectively. Due to the 3D geometric characteristics of the MJMs and the limitation of the depth of field in imaging, it is difficult to observe all the cells within the MJMs. We have collected a number of such MJMs and counted the number of four kinds of cells that are visible in sodium alginate MJMs, as shown in Fig. 6(b). Theoretically, the number of cells can be controlled by adjusting cell concentrations and flow rates of individual phases. Fig. 6(c) shows the fusion of bright field and fluorescence images of sodium alginate MJMs acquired after 7 days of co-culture. All the cells are stained with Hoechst dye to determine the cell death. According to Fig. 6(c), most of the cells are alive and proliferate within the alginate microgels when incubated in a fresh culture medium. Furthermore, all living cells grow into a 3D spherical cell mass after 7 days, as shown in the bottom right of Fig. 6(c). The results demonstrate the technical feasibility of 3D cell co-culture within sodium alginate MJMs fabricated by the MCFF process which would have potential applications for studying artificial organs. Despite the successful demonstration of 3D co-culture of four different cells, this *in vitro* experiment still has limitations. For example, it is difficult to differentiate among different cell types after 7 days of co-culture because all the cells are stained with Hoechst dye. Using different fluorescence markers may help distinguish among different cell types in the future. Besides, as a demonstration of the MCFF process in cell encapsulation, the selection of the cell types and the co-culture protocol are not optimized in this experiment. Further study is needed to demonstrate the interactions and synergistic effects of different cells within the MJMs. Regardless of these limitations, our study has already implied the technical feasibility of 3D co-culture of different cell types for potential applications in regeneration medicine.

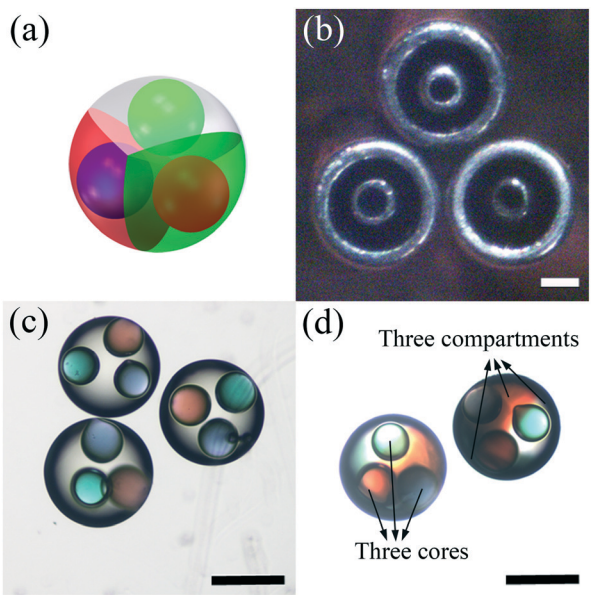

Fig. 7 Demonstration of fabricating MJMs with more than two compartments (scale bars: 300 μm): (a) schematic of three cores and three compartments integrated into a single MJM agent; (b) a picture of the needle assembly showing the combination of three coaxial needles; (c) microscopy image of the three-core microcapsules; (d) microscopy image of the MJMs with three compartments.

Fabrication of MJMs with three cores and three compartments

By increasing the number of coaxial needles in MCFF, we are also able to produce MJMs with more than two compartments, as illustrated in Fig. 7(a) where three cores and three compartments are integrated into a single MJM agent. Such a

three-compartment MJM agent is fabricated using the MCFF setup consisting of three parallel coaxial needles, as shown in Fig. 7(b). When the photocurable ETPTA solutions are used as the shell materials, the multicompartment double emulsions with three different cores can be fabricated by this method, as shown in Fig. 7(c). When two of the three outer phases of ETPTA solution are stained with green and red dyes, the morphology of resultant MJMs exhibits a complex structure, as indicated in Fig. 7(d). The core–shell configuration of the MJMs is also displayed in a video clip in the ESI† (S4). The volumetric flow rates of the three inner, three outer, and focusing streams are 3 ml h^{-1}, 20 ml h^{-1}, and 600 ml h^{-1}, respectively. It is worth noting that more complex Janus microcapsules with multiple cores and compartments can be generated in this MCFF method by employing much more coaxial needles, and the flow rates of different phases can be adjusted in a wide range to maintain the satisfactory morphology and internal topological structure. More importantly, the MCFF device can be easily scaled up to boost the throughput due to its simple geometry and low cost.

Conclusions

In summary, we have developed a novel MCFF process for single-step fabrication of MJMs with tunable morphological and structural characteristics, high throughput, and low cost. The MCFF process uses a simple experimental setup, involves liquid flow of moderate Reynolds number, and produces microdroplets dispersible in an open space. Therefore, it can be easily scaled up and integrated with other processes for mass production of MJMs in an industrial setting. By tuning the flow rates of different phases in the MCFF device, we are able to produce MJMs with different morphological and structural characteristics for different applications. We have produced magnetic MJMs and demonstrated the translational and rotational manipulations by an external magnetic field. Furthermore, multiple cells are encapsulated in sodium alginate MJMs for potential application of 3D cell co-culture. In addition, MJMs with more than two compartments have also been produced by increasing the number of coaxial needles. In summary, the MCFF process provides a versatile microfabrication platform to produce complex emulsions for potential applications such as micro-reactors,[42] photonic crystals,[43] drug release,[44] and cell encapsulation.[45]

Conflicts of interest

There are no conflicts to declare.

Acknowledgements

This work is supported by the National Natural Science Foundation of China (No. 11472270, 81327803 and 11621202) and the Fundamental Research Funds for the Central Universities.

References

1 F. Liang, C. Zhang and Z. Yang, *Adv. Mater.*, 2014, **26**, 6944–6949.
2 S. Lone and I. W. Cheong, *RSC Adv.*, 2014, **4**, 13322–13333.
3 T. Nisisako, *Curr. Opin. Colloid Interface Sci.*, 2016, **25**, 1–12.
4 C. X. Zhao, *Adv. Drug Delivery Rev.*, 2013, **65**, 1420–1446.
5 L. Adams, T. E. Kodger, S. H. Kim, H. C. Shum, T. Franke and D. A. Weitz, *Soft Matter*, 2012, **8**, 10719–10724.
6 C. Chen, A. R. Abate, D. Lee, E. M. Terentjev and D. A. Weitz, *Adv. Mater.*, 2009, **21**, 3201–3204.
7 A. Walther and A. H. Müller, *Chem. Rev.*, 2013, **113**, 5194–5261.
8 V. Rastogi, S. Melle, O. G. Calderon, A. A. García, M. Marquez and O. D. Velev, *Adv. Mater.*, 2008, **20**, 4263–4268.
9 H. Hwang, S. H. Kim and S. M. Yang, *Lab Chip*, 2011, **11**, 87–92.
10 F. Tu and D. Lee, *Chem. Commun.*, 2014, **50**, 15549–15552.
11 W. Zhang and X. He, *J. Biomech. Eng.*, 2009, **131**, 074515.
12 D. I. D. Cho and H. J. Yoo, *J. Microelectromech. Syst.*, 2015, **24**, 10–18.
13 L. Shang, F. Fu, Y. Cheng, H. Wang, Y. Liu, Y. Zhao and Z. Gu, *J. Am. Chem. Soc.*, 2015, **137**, 15533–15539.
14 H. Chen, Y. Zhao, J. Li, M. Guo, J. Wan, D. A. Weitz and H. A. Stone, *Lab Chip*, 2011, **11**, 2312–2315.
15 T. Nisisako, T. Torii, T. Takahashi and Y. Takizawa, *Adv. Mater.*, 2006, **18**, 1152–1156.
16 L. Zhao, L. Pan, K. Zhang, S. Guo, W. Liu, Y. Wang, Y. Chen, X. Zhao and H. Chan, *Lab Chip*, 2009, **9**, 2981–2986.
17 L. Shang, Y. Cheng, J. Wang, H. Ding, F. Rong, Y. Zhao and Z. Gu, *Lab Chip*, 2014, **14**, 3489–3493.
18 S. Kim, J. W. Shim and S. Yang, *Angew. Chem.*, 2011, **123**, 1203–1206.
19 J. Jeong, A. Gross, W. S. Wei, F. Tu, D. Lee, P. J. Collings and A. Yodh, *Soft Matter*, 2015, **11**, 6747–6754.
20 C. Choi, D. A. Weitz and C. Lee, *Adv. Mater.*, 2013, **25**, 2536–2541.
21 H. Chen, Y. Zhao, Y. Song and L. Jiang, *J. Am. Chem. Soc.*, 2008, **130**, 7800–7801.
22 S. Deshpande, Y. Caspi, A. E. Meijering and C. Dekker, *Nat. Commun.*, 2016, **7**.
23 H. C. Shum, Y. Zhao, S. Kim and D. A. Weitz, *Angew. Chem.*, 2011, **123**, 1686–1689.
24 C. Choi, D. A. Weitz and C. Lee, *Adv. Mater.*, 2013, **25**, 2536–2541.
25 L. D. Zarzar, V. Sresht, E. M. Sletten, J. A. Kalow, D. Blankschtein and T. M. Swager, *Nature*, 2015, **518**, 520–524.
26 T. Y. Lee, R. Praveenkumar, Y. K. Oh, K. Lee and S. H. Kim, *J. Mater. Chem. B*, 2016, **4**, 3232–3238.
27 L. Martín-Banderas, M. Flores-Mosquera, P. Riesco-Chueca, A. Rodríguez-Gil, Á. Cebolla, S. Chávez and A. M. Gañán-Calvo, *Small*, 2005, **1**, 688–692.
28 L. Martín-Banderas, A. Rodríguez-Gil, Á. Cebolla, S. Chávez, T. Berdún-Álvarez, J. M. Fernandez Garcia, M. Flores-Mosquera and A. M. Gañán-Calvo, *Adv. Mater.*, 2006, **18**, 559–564.

29 A. M. Gañán-Calvo, *Phys. Rev. Lett.*, 1998, **80**, 285.
30 T. Si, F. Li, X. Y. Yin and X. Z. Yin, *J. Fluid Mech.*, 2009, **629**, 1–23.
31 Z. Zhu, T. Si and R. X. Xu, *Lab Chip*, 2015, **15**, 646–649.
32 T. Si, H. Feng, X. Luo and R. X. Xu, *Microfluid. Nanofluid.*, 2015, **18**, 967–977.
33 G. Li, X. Luo, T. Si and R. X. Xu, *Phys. Fluids*, 2014, **26**, 054101.
34 L. Shang, Y. Cheng, J. Wang, Y. Yu, Y. Zhao, Y. Chen and Z. Gu, *Lab Chip*, 2016, **16**, 251–255.
35 L. Shang, F. Fu, Y. Cheng, H. Wang, Y. Liu, Y. Zhao and Z. Gu, *J. Am. Chem. Soc.*, 2015, **137**, 15533–15539.
36 Y. S. Kang, S. Risbud, J. F. Rabolt and P. Stroeve, *Chem. Mater.*, 1996, **8**, 2209–2211.
37 S. H. Hu, C. H. Tsai, C. F. Liao, D. M. Liu and S. Y. Chen, *Langmuir*, 2008, **24**, 11811–11818.
38 M. Arruebo, R. Fernández-Pacheco, M. R. Ibarra and J. Santamaría, *Nano Today*, 2007, **2**, 22–32.
39 Y. Komazaki, H. Hirama and T. Torii, *J. Appl. Phys.*, 2015, **117**, 154506.
40 J. Weizenecker, B. Gleich, J. Rahmer, H. Dahnke and J. Borgert, *Phys. Med. Biol.*, 2009, **54**, L1.
41 B. Zebli, A. S. Susha, G. B. Sukhorukov, A. L. Rogach and W. J. Parak, *Langmuir*, 2005, **21**, 4262–4265.
42 W. J. Duncanson, A. Abbaspourrad, H. C. Shum, S.-H. Kim, L. L. Adams and D. A. Weitz, *Langmuir*, 2012, **28**, 6742–6745.
43 Y. Zhao, Z. Xie, H. Gu, L. Jin, X. Zhao, B. Wang and Z. Gu, *NPG Asia Mater.*, 2012, **4**, e25.
44 J. Liu, C. Detrembleur, S. Mornet, C. Jérôme and E. Duguet, *J. Mater. Chem. B*, 2015, **3**, 6117–6147.
45 W. Zhang, S. Zhao, W. Rao, J. Snyder, J. K. Choi, J. Wang, I. A. Khan, N. B. Saleh, P. J. Mohler and J. Yu, *J. Mater. Chem. B*, 2013, **1**, 1002–1009.